THE ROYAL SOCIETY

High-resolution X-ray diffraction analyses of protein crystals

By H. M. Volz[1] and R. J. Matyi[2]

[1]*Materials Science Program,* [2]*Department of Materials Science and Engineering, University of Wisconsin, Madison, WI 53706, USA*

High-resolution triple-axis X-ray diffraction analyses have been performed on tetragonal crystals of hen egg-white lysozyme (HEWL). In order to perform these analyses in a laboratory setting, an X-ray optical system consisting of a pair of parabolic graded X-ray mirrors and an asymmetric channel-cut crystal was employed. Analyses of thin silicon crystals confirmed the differences between the transmission geometry used for the HEWL crystals and the more common reflection geometry typically used for the characterization of inorganic crystals. Significant differences in the intensity distribution in the vicinity of the HEWL reciprocal lattice points between different reflections of the same crystal and between different crystals have been observed.

Keywords: triple-axis X-ray diffraction; protein crystals; reciprocal space mapping

1. Introduction

Some of the earliest applications of X-ray methods for the analysis of defects in crystals were made on naturally occurring materials. Lang's pioneering studies of diamond (Lang 1974) and quartz (Lang 1967) demonstrated the value of X-ray analytical techniques in relating the crystal's natural growth conditions to the resultant grown-in defect structure.

Over the last two decades in the semiconductor industry, much progress has been made in understanding the generation of defects during single-crystal growth. Through techniques such as high-resolution X-ray diffraction, information about crystalline quality can be readily obtained, which is then rapidly fed back to crystal-growth laboratories. As a result, semiconductors are now routinely grown with defect densities that can approach zero.

But in contrast with state-of-the-art semiconductor crystal growth, protein crystallization is more of an art form. Reproducibility is a problem, and 'large' single crystals are typically less than 1 mm^3. Most importantly, the structural quality of protein crystals is considerably lower than that of modern semiconductor materials. X-rays are used extensively by protein crystallographers, but usually only for structural determination; however, the accuracy of these structural analyses is adversely affected by the large number of defects in protein crystals (McPherson 1989).

Despite their benefit to the inorganic crystal-growth community, there have been relatively few high-resolution X-ray diffraction analyses of protein crystals. One of the earliest systematic analyses of X-ray rocking curves from protein crystals was performed by Shaikevitch & Kam (1981). Using slit-collimated radiation from a sealed X-ray tube, they reported a mosaic spread of *ca.* 60 arc seconds for a lysozyme crystal

at $2\theta \approx 15°$. Recently, the advent of synchrotron sources with intense radiation and low divergence has led to a number of other X-ray rocking-curve analyses (Fourme *et al*. 1995; Helliwell 1988; Colapietro *et al*. 1992; Snell *et al*. 1995). Rocking-curve full widths at half maximum (FWHM) as narrow as 8.3 arc seconds (0.0023°) from the (776) reflection have been reported for lysozyme crystals grown in microgravity (Snell *et al*. 1995). This value is far superior to the *ca*. 47 arc seconds FWHM observed in a similar crystal grown on Earth. X-ray topographic studies employing synchrotron radiation have been reported recently by Fourme *et al*. (1995), Izumi *et al*. (1996), Stojanoff & Siddons (1996) and Stojanoff *et al*. (1997), which include both perfect crystal monochromated topographs (Fourme *et al*. 1995; Stojanoff & Siddons 1996; Stojanoff *et al*. 1997) and white-beam topographs (Izumi *et al*. 1996; Stojanoff & Siddons 1996; Stojanoff *et al*. 1997). In all cases defects in lysozyme crystals were observed, but unambiguous defect assignments were difficult. This is often true of topographic images of structurally defective crystals. The work by Stojanoff and coworkers did demonstrate, however, that a decrease in the defect density as observed through topographic imaging did correlate with an increase in structural resolution in subsequent crystallographic analyses (Stojanoff & Siddons 1996; Stojanoff *et al*. 1997).

The goal of the present work is to apply techniques of high-resolution X-ray diffraction (specifically, the reciprocal space mapping developed primarily for semiconductor materials) to the analysis of protein crystals. Ultimately, these analyses are expected to lead to a better understanding of the conditions that limit structural quality in protein crystal growth. Characterization of grown-in defects could lead to methods of reducing their densities, thereby increasing crystalline quality and improving the structural determinations that are central to the study of protein function.

In the following investigation, we have modified an X-ray diffraction apparatus previously used for semiconductor analyses to handle protein crystals. Interestingly, one consequence of the different physical properties of semiconductor and protein samples is different X-ray geometries. With the exception of occasional studies such as those by Zaumseil & Winter (1982) and by Gartstein & Cowley (1990), semiconductor reciprocal space maps are almost always performed in reflection. In contrast, the small size and low X-ray absorption characteristics of protein crystals make them more amenable to transmission. It should be noted that many of Lang's X-ray studies were performed in transmission geometries; the significance of this will become apparent below.

The protein chosen for study was hen egg-white lysozyme (HEWL), which is a well-characterized protein frequently used in crystal-growth studies, due in part to its relative ease of crystallization.

2. Experimental

Samples of crystallized HEWL were obtained from Professor H. Holden and Dr J. Thoden of the Institute for Enzyme Research at the University of Wisconsin, Madison. Crystals were grown by microdialysis, a liquid–liquid diffusion technique. The lysozyme starting material was obtained from Sigma Chemical, and the concentration used was 40 mg ml^{-1} in water. Dialysis was performed at pH 4.7 using 20 mM

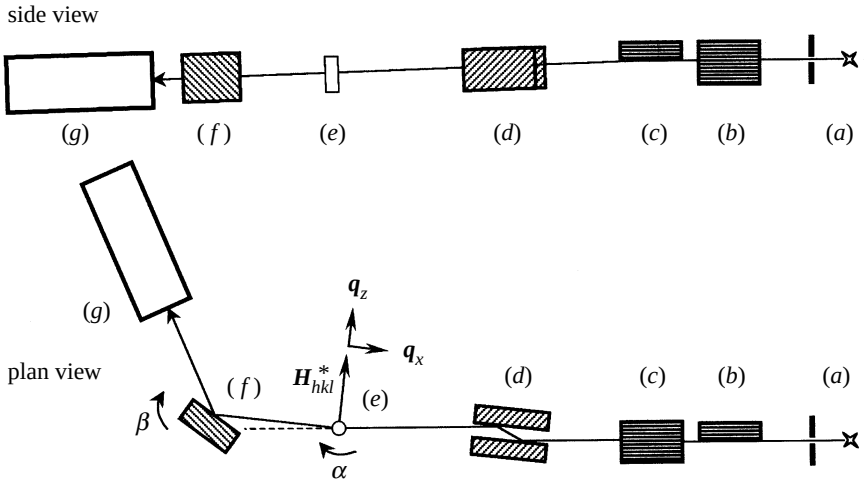

Figure 1. Schematic illustration of the X-ray optical system used in the current study: (*a*) X-ray source; (*b*) horizontal mirror; (*c*) vertical mirror; (*d*) asymmetric channel-cut collimator; (*e*) sample; (*f*) analyser; (*g*) detector. The plan view also shows the angular deviations of the sample (α) and analyser (β) crystals, the orientation of the reciprocal lattice vector $\boldsymbol{H}^*_{hkl}$ in the transmission geometry, and the sense of the deviation vectors $\boldsymbol{q}_x$ and $\boldsymbol{q}_z$.

sodium acetate and 850 mM sodium chloride. Crystals of appreciable size typically grew within two days.

The samples used in this study were tetragonal (space group $P4_32_12$) with {110} facets clearly visible. Each optically transparent crystal was mounted in a 0.5 mm glass capillary, whose ends were then sealed with wax before mounting with modelling clay on a eucentric goniometer. Unit cell parameters, $a = 79.35$ Å and $c = 38.07$ Å, were determined at room temperature using a Siemens P4RA diffractometer equipped with a Hi-Star X-1000 multiwire detector. Cu-$K\alpha$ X-rays were obtained from a Siemens rotating anode generator equipped with a graphite monochromator.

Transmission X-ray rocking curves and reciprocal space maps were recorded with a Huber 424/511 four-circle diffractometer modified with TECO stepper motors to permit a minimum step size of 0.001 25° (4.5 arc seconds). Figure 1 illustrates the X-ray optical system that was used for this study. The Cu-$K\alpha$ X-rays were generated by a Rigaku RU-200 rotating anode generator configured with a point focus from a 0.5 mm × 10 mm focal spot. The incident X-rays were conditioned by a crossed pair of parabolic graded X-ray mirrors (Osmic, Inc., Troy, MI, USA). The crossed mirrors, which were situated in a novel X-ray optical system (Matyi *et al.* 1999), produced a quasi-parallel X-ray beam (nominally three arc minutes horizontal and vertical divergence) with an approximate beam dimension of 1 mm × 1 mm. The use of this crossed-mirror beam conditioner resulted in a significant increase in the incident beam X-ray flux as well as a two-dimensional collimation of the incident beam. Both effects were advantageous for the analysis of small weakly diffracting HEWL crystals in a conventional laboratory setting.

Following conditioning by the crossed parabolic mirrors, the incident X-ray beam was further refined by diffraction from a grooved silicon crystal supplied by Bede Scientific. The two asymmetric (220) reflections served to condition the horizontal

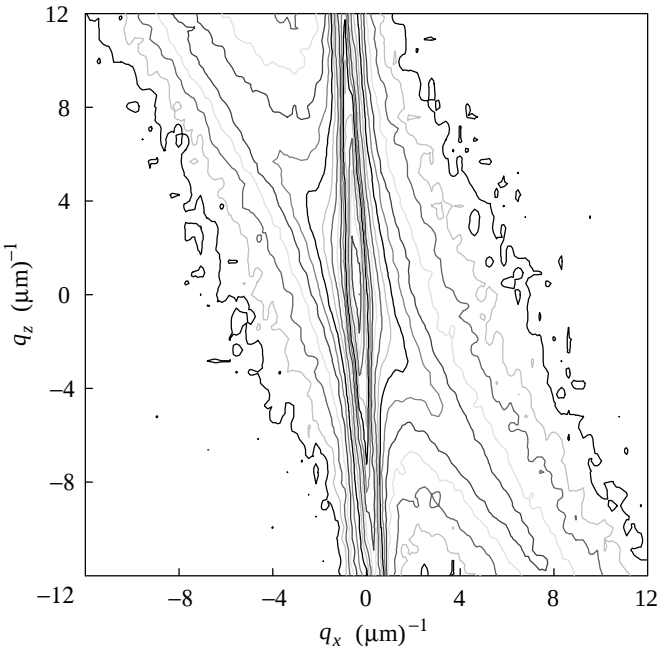

Figure 2. 004 reciprocal space map from a bulk GaAs crystal recorded using the incident beam conditioner illustrated in figure 1.

divergence of the X-ray beam from three arc minutes to several arc seconds; the use of an asymmetric groove significantly increased the transmitted X-ray flux (Loxley *et al*. 1995). The conditioned incident beam was then diffracted in transmission geometry from a HEWL crystal, and the diffracted beam was analysed by a single (004) reflection from a highly perfect Ge [001] single crystal. Reciprocal space scans of specific reflections were obtained by performing θ–2θ scans with an increment in the sample angular position between scans.

The angular (diffractometer) coordinates were converted to orthogonal deviations (q_x, q_z) from the exact Bragg condition in reciprocal space using the relations

$$q_x = (2\alpha - \beta)(\sin\theta/\lambda), \qquad q_z = \beta(\cos\theta/\lambda) \tag{2.1}$$

where α and β are, respectively, the deviations of the sample and analyser crystals from the exact Bragg condition in radians. As shown in figure 1, $\boldsymbol{q}_z$ and $\boldsymbol{q}_x$ correspond to directions that are, respectively, parallel and perpendicular to the reciprocal lattice vector for a particular Bragg reflection.

Due to the unconventional beam conditioning employed in this study, some preliminary analyses were performed on well-characterized materials. Figure 2 illustrates the 004 reciprocal space map that was recorded from a [001] GaAs bulk crystal in reflection geometry. This reciprocal space map (as well as those presented below) is plotted with contours of the logarithm of intensity, with each contour level representing $10^{0.25}$ counts per second (i.e. four contours per decade of intensity).

Figure 2 shows the 004 crystal truncation rod (or 'surface streak') in the [004] direction that is commonly observed in high-resolution reciprocal space maps from highly perfect crystals. In addition, an intense angled streak of X-ray intensity is also

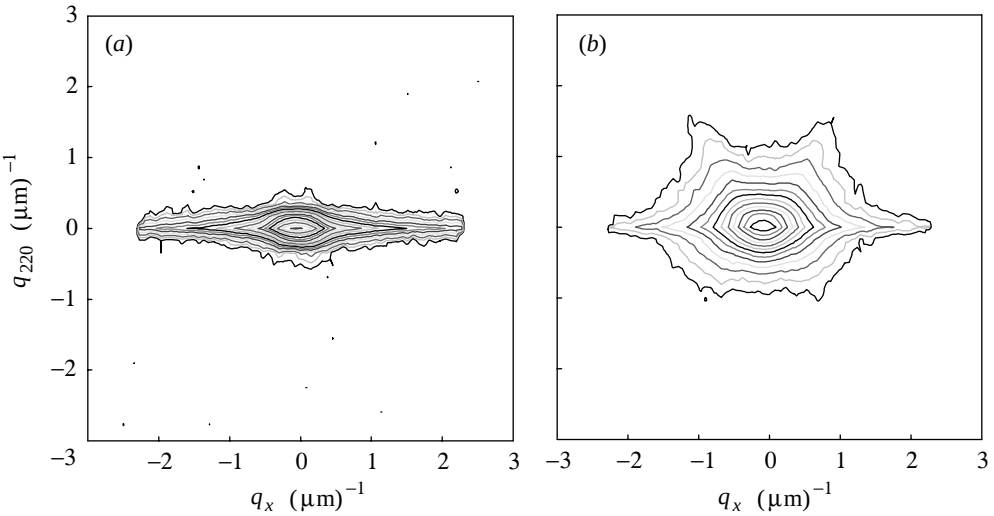

Figure 3. 220 reciprocal space maps from thin (*ca.* 60 μm thick) silicon samples: (*a*) unannealed; (*b*) annealed (see text for details).

seen. We attribute this feature to the extremely high incident intensity that was generated by the crossed-mirror beam conditioner. An analysis of the X-ray data showed that the reciprocal coordinates of the streak corresponded to the angular position of the sample when it satisfied the Bragg condition, regardless of the angular setting of the analyser crystal. We believe that the highly intense diffracted beam from the sample, propagating towards the analyser, generated parasitic intensity due to air scatter in our diffractometer system. As noted elsewhere (Matyi 1992), air scatter from an intense diffracted beam will create parasitic intensity in a reciprocal space map that is coincident with the 'analyser streak' that might be expected from a single-reflection analyser crystal. The off-peak intensity streak remains above background over an angular range that is many times greater than the intrinsic reflecting range of the Ge (004) analyser crystal used in this work, suggesting that this feature is not the 'analyser streak'. Subsequent analyses employed extensive shielding of the detector with lead foils to minimize the contamination of this parasitic scatter.

3. Results

As noted above, unlike high-resolution reciprocal space mapping of materials such as most bulk and thin-film semiconductors, our studies of HEWL crystals would be conducted in a transmission geometry. However, because of the relative scarcity of examples in the literature of high-resolution diffraction analyses in the transmission geometry, we felt that it would be prudent to examine a model system first. Since the precipitation of oxygen in Czochralski silicon yields a well-known defect structure, it was decided that this would be an excellent test of reciprocal space mapping in the transmission geometry. Figure 3 shows transmission 220 reciprocal space maps recorded from samples of silicon that had been subjected to various thermal processes in order to produce different levels of oxygen precipitation (Shaffner *et al*. 1985). The samples were thinned to *ca.* 60 μm (resulting in $\mu t \approx 1$, where μ is the linear X-ray absorption coefficient and t is the sample thickness) by mechanical polishing and

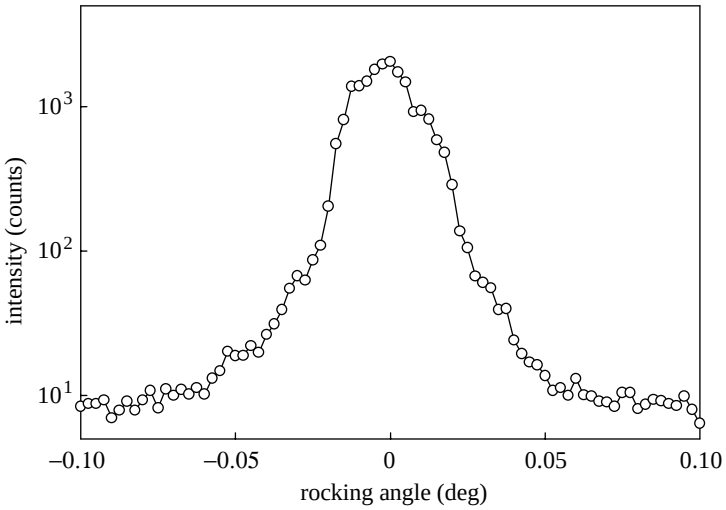

Figure 4. Double-axis rocking curve from HEWL crystal A.

chemical etching in order to permit transmission diffraction analyses. The reciprocal space maps from these silicon samples were recorded using a Bede 150 double-axis diffractometer modified for high-resolution triple-axis measurements (Matyi 1992).

Prior analyses of these silicon samples by scanning Lang topography (Shaffner *et al*. 1985) had confirmed an increase in the concentration of oxygen precipitates as the annealing time was increased. Figure 3 shows that the unannealed sample (initial interstitial oxygen concentration 36 parts per million (ppm)) generated significant scattering only perpendicular to the [220] direction. Annealing at 750 °C for 15 h followed by 1050 °C for 8 h decreased the interstitial oxygen concentration to 9 ppm. The accompanying increase in the concentration of oxygen precipitates resulted in enhanced diffuse scatter in the vicinity of the 220 reciprocal lattice point with significant anisotropy.

These observations can be understood by considering the diffraction geometry in reciprocal space for symmetric-transmission Laue diffraction. In contrast with the more common reflection geometry, the reciprocal lattice vector for a symmetric reflection in the transmission case will be parallel to the surface. Any effects of the truncation of the crystal lattice at the surface will therefore be manifested in a direction that is perpendicular to the reciprocal lattice vector. Diffraction patterns in transmission electron microscopy (TEM) are sensitive to the 'shape function' of a crystal in which the size of a diffraction spot in a given direction is inversely proportional to the sample thickness in that direction. However, both our silicon samples and the HEWL crystals (discussed below) are far thicker than conventional TEM samples. We therefore expect that, in our X-ray analyses, the broadening of a reciprocal lattice point in the direction perpendicular to a surface will be dominated by the well-known q^{-2} dependence that accompanies the Fourier transform of a semi-infinite step function (i.e. the truncation of a bulk three-dimensional crystal by a surface).

The broadening due to the truncation at the crystal surface introduces an important difference between the reflection and transmission geometries. In the former case, non-uniform strains in the crystal (resulting in changes in the length of a reciprocal

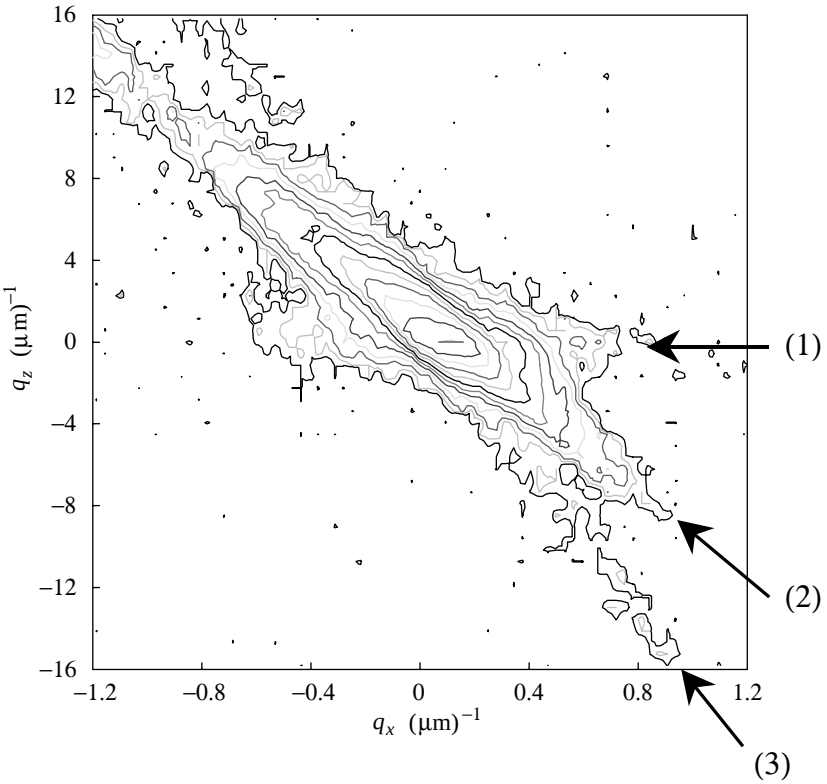

Figure 5. Triple-axis reciprocal space map from HEWL crystal A (see text for details).

lattice vector) will result in extra X-ray intensity *parallel* to the surface streak, while the effects of mosaic spread or misorientations will broaden the intensity distribution *perpendicularly*. In the transmission-geometry case, this will be reversed: mosaic spread will be coincident with the direction of the surface streak (if one is present) *perpendicular* to the reciprocal lattice vector, while strains will be represented by intensity in the orthogonal direction, *parallel* to the reciprocal lattice vector.

It is now possible to rationalize the results from the silicon samples. We do not believe that the single horizontal streak seen in the unannealed sample (figure 3*a*) is analogous to the 'shape factor' commonly seen in TEM, since the 60 μm sample thickness would yield a streak length of $2\pi/t$ or *ca.* 0.1 μm^{-1}. This is much smaller than the extent of the streak that was observed experimentally. Instead, we believe that this transverse intensity feature is due to either a mosaic spread (possibly arising from the extensive polishing needed to thin the sample), the surface streak due to the truncation of the crystal at the entrance and exit faces as discussed above, or both.

In the case of the annealed sample (figure 3*b*) we again observe the transverse streak; in addition, we also observe enhanced anisotropic diffuse scatter in specific directions in the positive q-direction. These results are consistent with the presence of preferentially oriented oxygen precipitates generating non-uniform compressive strains in the host silicon lattice (Shaffner *et al*. 1985). This interpretation is in good agreement with the results of Zaumseil & Winter (1982).

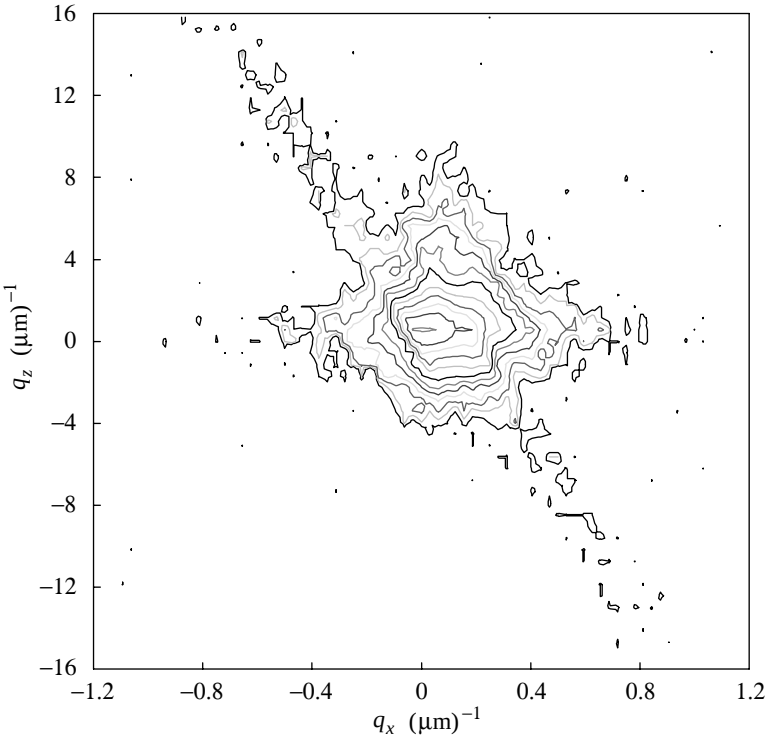

Figure 6. A second reciprocal space map from HEWL crystal A using a different reflection.

Two HEWL crystals were then selected for analysis by transmission high-resolution diffraction. Figure 4 illustrates a double-axis rocking curve that was recorded from one HEWL crystal examined in this study (herein referred to as crystal A). Due to the large size of the HEWL unit cell, the Bragg angle of this reflection is relatively small ($\theta_B = 3.16°$); this Bragg angle is consistent with a {440} reflection. The measured FWHM of the rocking curve is 77 arc seconds, in good agreement with other rocking-curve analyses of HEWL crystals (Fourme *et al*. 1995).

The corresponding reciprocal space map from crystal A is shown in figure 5. Although the data are plotted in the same units of reciprocal micrometres, the horizontal axis (perpendicular to the reciprocal lattice vector direction) has been expanded to aid in reading the figure. The reason for the different coordinate magnitudes, despite comparable angular ranges scanned experimentally, lies in the nature of the geometric transformation given in equation (2.1), where the trigonometric sine of the Bragg angle will be considerably less than the cosine of that angle at for small Bragg angles.

Even with this geometric distortion, figure 5 exhibits an irregular intensity distribution that is reminiscent of highly defective semiconductor crystals. Specifically, in the figure one can observe: (1) a faint distribution of intensity in the transverse direction (i.e. horizontally in the figure); (2) an inclined relatively intense distribution extending from the upper left and through the reciprocal lattice point towards the lower right; and (3) a weaker intensity distribution also extending from upper left to lower right in the figure, but at a steeper angle.

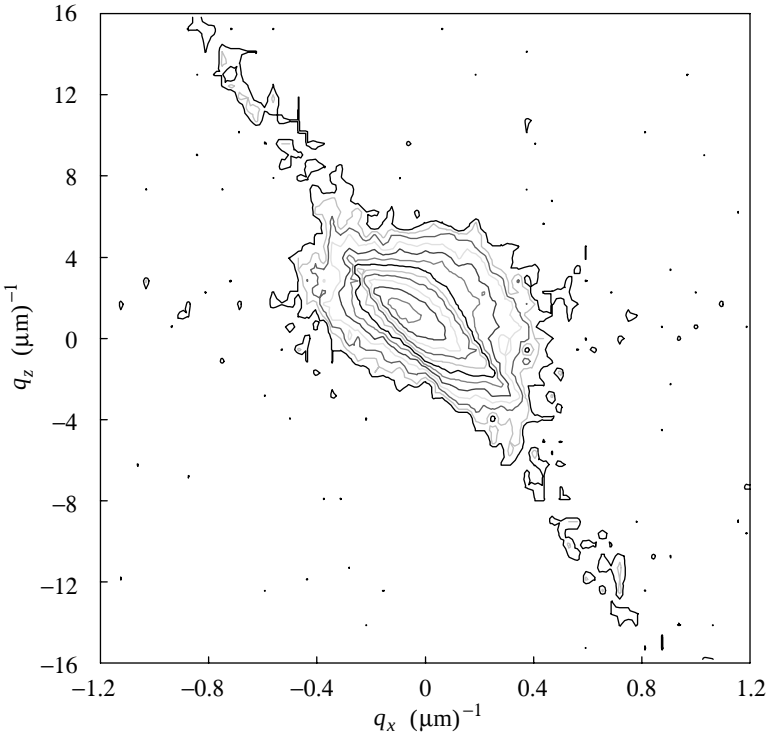

Figure 7. Triple-axis reciprocal space map from HEWL crystal B.

We believe that this third intensity feature is the signature of parasitic scattering from our X-ray optical system superimposed on a possible analyser streak. This feature is evident in all reciprocal space maps recorded from other reflections as well as other crystals (as demonstrated below) and always appears at an angle θ_B from the vertical. The origin of the other, more intense, inclined feature (number (2) on the figure) is unknown at the present time. While it is tempting to identify it as an inclined surface streak, any such conclusion would be speculative without further optical and X-ray analyses of this crystal. Given the thickness of the crystal, we do not believe that this feature can be a manifestation of the crystal's shape function. Finally, we believe that the horizontal intensity distribution (number (1) on the figure) is likely to be due to the mosaic distribution in the HEWL crystal. If this interpretation is correct, then the mosaic spread of the crystal would be *ca.* 150–180 arc seconds, a reasonable value for HEWL crystals.

We found that it was a relatively straightforward matter to locate and record other reflections with a simple ϕ-rotation of the crystal in the four circle diffractometer. Figure 6 illustrates a second reciprocal space map recorded from crystal A. Once again, the measured Bragg angle of this second reflection was 3.16° and is thus consistent with a {440} reflection. However, the difference between the two reciprocal space maps is striking, with the only similarities being the inclined parasitic intensity from the crossed-mirror beam conditioner and the horizontal intensity distribution that we tentatively attribute to mosaic spread. We note that in figure 6 there is significant intensity distributed longitudinally (in the direction of the reciprocal lattice

vector, or vertically in the figure) indicating likelihood of a compressive strain in the crystal. Further study is needed to understand the origin of this unexpected intensity distribution and to rationalize the differences seen in the reciprocal space maps from different reflections from the same HEWL crystal.

Figure 7 shows a reciprocal space map recorded from a second HEWL crystal (denoted crystal B). This crystal was grown under nominally identical conditions as those used for crystal A, although it did exhibit a larger {110} growth facet. The FWHM of the double-axis rocking curve from crystal B was only 54 arc seconds. The intensity distribution in its reciprocal space map is much more isotropic than was observed in the first crystal, suggesting a higher level of structural perfection. Again, further analyses will be needed to confirm that this is indeed the case.

4. Conclusions

This work has demonstrated that high-resolution X-ray reciprocal space mapping, a widely used technique for the characterization of semiconductor crystals, can be successfully applied to more structurally imperfect protein crystals. It should be noted that all of this work was done in a conventional laboratory environment; the use of a synchrotron source is not required. Future work will concentrate on better understanding the intensity distribution seen in the transmission geometry from protein crystals with varying degrees of structural perfection, and on relating the observed defect characteristics to the variables in the protein crystal-growth process.

The authors are grateful to Professor H. Holden and Dr J. Thoden of the Institute for Enzyme Research at the University of Wisconsin–Madison for supplying the HEWL crystals used in this study, to Professor D. Rich of the School of Pharmacy for assistance in determining the unit cell constants of the crystals studied, and to Mr K. Matney of Bede Scientific, Inc., for the use of the asymmetric channel-cut silicon crystal. We are also grateful to Dr R. Deslattes (NIST) and Dr A. Chernov (NASA) for discussions that led to the inception of this work. Support for one of us (H.M.V.) came from an NSF Graduate Fellowship, while support for the construction of the crossed-mirror system came from the NSF under grant DMR-9319421.

References

Colapietro, M., Cappuccio, G., Marciante, C., Pifferi, A., Spagna, R. & Helliwell, J. R. 1992 *J. Appl. Crystallogr.* **25**, 192.

Fourme, R., Ducruix, A., Ries-Kautt, M. & Capelle, R. 1995 *J. Synch. Rad.* **2**, 136.

Gartstein, E. L. & Cowley, R. A. 1990 *Acta Crystallogr.* A **46**, 576.

Helliwell, J. R. 1988 *J. Cryst. Growth* **90**, 259.

Izumi, K., Sawamura, S. & Ataka, M. 1996 *J. Cryst. Growth* **168**, 106.

Lang, A. R. 1967 *J. Phys. Chem. Solids* **28**, 833.

Lang, A. R. 1974 *J. Cryst. Growth* **24/25**, 108.

Loxley, N., Tanner, B. K. & Bowen, D. K. 1995 *Adv. X-ray Analysis* **38**, 361.

McPherson, A. 1989 *Preparation and analysis of protein crystals.* Malabar, FL: Krieger.

Matyi, R. J. 1992 *Rev. Sci. Instrum.* **63**, 5591.

Matyi, R. J., Moran, P. D., Hagquist, W. D. & Volz, H. M. 1999 *Rev. Sci. Instrum.* (Submitted.)

Shaffner, T. J., Matyi, R. J., Stephens, A. E. & Meyer, F. O. 1985 *Electrochem. Soc. Ext. Abs.* Issue no. 85-2, p. 482.

Shaikevitch, A. & Kam, Z. 1981 *Acta Crystallogr.* A **37**, 871.

Snell, E. H., Weisgerber, S., Helliwell, J. R., Weckert, E., Hölzer, K. & Schroer, K. 1995 *Acta Crystallogr.* D **51**, 1099.

Stojanoff, V. & Siddons, D. P. 1996 *Acta Crystallogr.* A **52**, 498.

Stojanoff, V., Siddons, D. P., Monaco, L. A., Vekilov, P. & Rosenberger, F. 1997 *Acta Crystallogr.* D **53**, 588.

Zaumseil, P. & Winter, U. 1982 *Physica Status Solidi* A **73**, 455.